Received: 5 November 2019 | Revised: 5 February 2020 | Accepted: 23 February 2020

DOI: 10.1002/prot.25885

RESEARCH ARTICLE

PROTEINS WILEY

# Kinetics of pH-dependent interactions between PD-1 and PD-L1 immune checkpoint proteins from molecular dynamics

Konstantin Klyukin[1] | Vitaly Alexandrov[1,2]

[1]Department of Chemical and Biomolecular Engineering, University of Nebraska-Lincoln, Lincoln, Nebraska

[2]Nebraska Center for Materials and Nanoscience, University of Nebraska-Lincoln, Lincoln, Nebraska

**Correspondence**
Vitaly Alexandrov, University of Nebraska-Lincoln, Lincoln, NE 68588.
Email: valexandrov2@unl.edu

**Funding information**
University of Nebraska-Lincoln

## Abstract

Immune checkpoint blockade of signaling pathways such as PD-1/PD-L1 has recently opened up a new avenue for highly efficient immunotherapeutic strategies to treat cancer. Since tumor microenvironments are characterized by lower pH (5.5-7.0), pH-dependent protein-ligand interactions can be exploited as efficient means to regulate drug affinity and specificity for a variety of malignancies. In this article, we investigate the mechanism and kinetics of pH-dependent binding and unbinding processes for the PD-1/PD-L1 checkpoint pair employing classical molecular dynamics simulations. Two representative pH levels corresponding to circumneutral physiological conditions of blood (pH 7.4) and acidic tumor microenvironment (pH 5.5) are considered. Our calculations demonstrate that pH plays a key role in protein-ligand interactions with small pH changes leading to several orders of magnitude increase in binding affinity. By identifying the binding pocket in the PD-1/PD-L1 complex, we show a pivotal role of the His68 protonation state of PD-1in the complex stabilization at low pH. The results on the reaction rate constants are in qualitative agreement with available experimental data. The obtained molecular details are important for further engineering of binding/unbinding kinetics to formulate more efficient immune checkpoint blockade strategies.

**KEYWORDS**

checkpoint blockade, molecular dynamics, protein binding affinity

## 1 | INTRODUCTION

Cancer cells can dampen or circumvent immune responses by activation of inhibitory checkpoint proteins. It was demonstrated that such immune-privileged microenvironment can be destroyed and antitumor function of immune cells can be restored through blocking the interaction between cancer and immune cell proteins.[1-4] This approach (a.k.a. immune checkpoint blockade) has recently revolutionized cancer immunotherapy leading to several FDA-approved drugs and was celebrated by the 2018 Nobel Prize in Medicine. Being a giant leap forward in cancer treatment, immune checkpoint blockade is one of the most prominent examples of enormous variability in patient responses to therapeutics. A fraction of patients even with metastatic tumors eliciting continued durable disease control has grown in recent years across a number of malignancies, but durable responses are still limited to a minority of patients.[4-6] Although fundamental causes for a huge range of therapeutic sensitivity are the subject of intense research, mechanistic understanding of checkpoint blockade and reasons for tumor immune rejection are still lacking being significantly outpaced by clinical research.

At the microscopic level, specifics of molecular interactions between checkpoint proteins and drugs should play an important role in defining the magnitude of immune response and drug resistance among patients. Among various factors controlling protein functions in tissues, the pH level is a key variable that can strongly affect receptor-ligand binding. On the molecular level, not only pH changes define the protonation state of amino acid residues, but also it may induce important conformational transitions affecting stability of protein complexes.[7-9] Since low pH (5.5-7) is one of the hallmarks of tumor microenvironment, pH-dependent receptor-ligand interactions

  

can be utilized to regulate binding/unbinding mechanisms and drug residence times in checkpoint blockade.

Prior experiments have indeed demonstrated the prominent role of reaction pH on binding affinity, for example, for antibodies against the IL-6 receptor at pH 6.0-7.4.[10,11] Another critical aspect translating to specificity of protein binding is protein mutations that can lead to modified interactions at the protein/ligand interface. For instance, it was revealed that only a single amino acid substitution (A132L) in the immune checkpoint programmed cell death protein-1 (PD-1) results in additional van der Waals contacts with its ligands PD-L1 and PD-L2 enhancing the binding affinity by 45- and 30-fold, respectively, compared to the wild type.[12] The presence of up to 10 amino acid substitutions was demonstrated to lead to a binding enhancement as large as 40 000-fold.[13] Full realization of such an outstanding tuning capacity for immune system activation through inhibition of checkpoints requires more detailed atomistic understanding of the role of specific protein-ligand interactions underlying checkpoint blockade. This knowledge will constitute a molecular basis for guiding the development of selective pH-dependent immune-modulating agents against cancer with milder adverse effects.

In this study, we elucidate the molecular details of pH-dependent binding and unbinding processes between PD-1 and PD-L1 that emerged as key targets for checkpoint blockade. To this end, we carry out a series of classical molecular dynamics (MD) simulations employing a combination of enhanced free-energy sampling techniques (metadynamics and umbrella sampling) to assess free energy barriers and associated rate constants for both binding and unbinding reactions. The obtained results qualitatively agree with recent experiments examining binding interactions between the high-affinity consensus (HAC) PD-1 mutant and its ligand PD-L1 as a function of pH.[13]

## 2 | COMPUTATIONAL METHODOLOGY

To model interactions between the HAC PD-1 and PD-L1 proteins,[13] we used the 5IUS crystal structure from Protein Data Bank. The missing residues, including protein tails and the PD1.86-88 loop, were recovered using the Modeller software.[14] As we show below, these residues are located far from the binding pocket and therefore are not directly involved in binding/unbinding reaction. Since the C2 domain of the PD-L1 protein also does not participate in binding with PD-1, residues 133-229 were removed (see Figure 1) to decrease the simulation cell size. The resulting complex was found to be stable and the initial binding pose is preserved after equilibration in an aqueous environment according to the root mean square displacement of heavy atoms as discussed below. The protonation state under certain pH value was determined using PropKa 3.1 package.[15] All MD simulations were carried out using the Gromacs 2016.3 simulation package[16] with Amber03 force field.[17]

The proteins were solvated with ~17 000 TIP3P water molecules in a rectangle box, resulting in ~55 700 atoms in total. The long-range electrostatic interactions were calculated by the means of the particle mesh Ewald decomposition algorithm. Cutoffs of 10 Å for electrostatic and vdW interactions were used to perform calculations with periodic boundary conditions. All hydrogen bonds were constrained using the LINCS algorithm allowing a simulation time step of 2 fs. The V-rescale thermostat[18] and Parrinello-Rahman pressure coupling[19] were applied during simulations to maintain temperature of 300 K and 1 bar pressure. The system geometry was first optimized until the forces become less than 1000 kJ/mol/nm. Then, the system was gradually heated from 0 to 300 K in the NVT ensemble with constrained solute atoms during 1 ns, after which the system underwent an NPT simulation of 20 ns for equilibration. After equilibration, the system was simulated using the NPT ensemble for 100 ns.

Infrequent metadynamics simulations were employed to estimate unbinding reaction rates ($k_{off}$) as implemented in the PLUMED 1.3 package.[20] The approach is based on the periodic biasing of collective variables (CVs) in order to increase the probability of transitions between metastable states.[21] We use the solvation state of binding pocket (the number of water molecules forming hydrogen bonds with the active sites listed in Table 1) and the center-of-mass distance between binding pocket of protein and its ligand as CVs to run well-tempered metadynamics simulations. The Gaussian hills were added every 8 ps with an initial height of 1.8 kJ/mol, width of 0.02 and 0.05

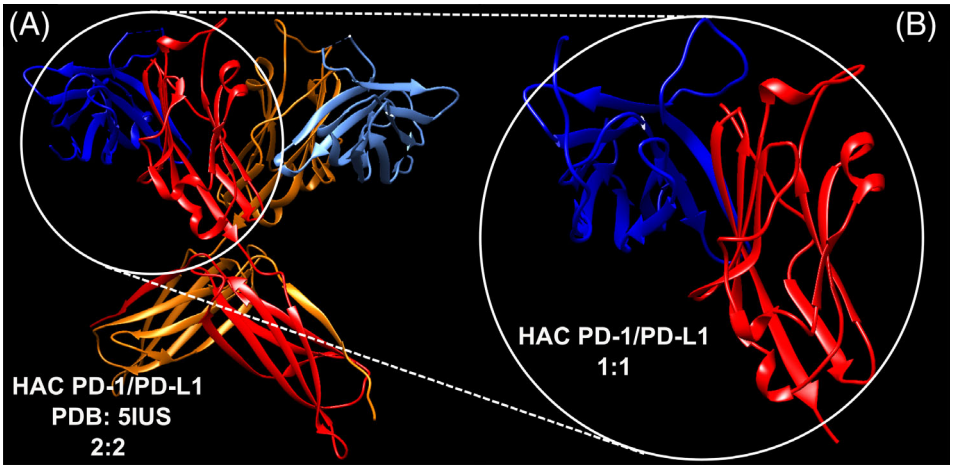


**FIGURE 1** A, Crystal structure (PDB ID: 5IUS) of the HAC PD-1/PD-L1 complex with a 2:2 binding stoichiometry[13] and (B) solution structure with a 1:1 binding stoichiometry used in the present work as a structural model for molecular dynamics simulations

for distance and solvation state CVs, correspondingly, and a bias factor of 10. These computational parameters are similar to several previous biomolecular modeling studies of unbinding kinetics employing the infrequent metadynamics formalism.[21] Several independent simulations were carried out to collect statistics and decrease uncertainty. The binding and unbinding rates were estimated assuming that its characteristic time follows a Poisson distribution. The unbinding time was directly calculated from metadynamics trajectories and corrected using the acceleration factor $e^{V(s,t)/KT}$, where $V(s,t)$ is the time-dependent bias potential. A similar computational scheme to calculate binding/unbinding kinetics has been recently applied in a number of works.[22,23] The binding barriers $\Delta G_{on}$ were estimated based on the first crossing between the bound and unbound states (USs). The US was defined as a state with a distance between PD-l and PD-L1 exceeding ~1.1 and ~1.2 nm for blood and acidic pH, correspondingly. The average $\Delta G_{on}$ value was calculated based on several independent trajectories, and the uncertainty was determined using standard error analysis.

**TABLE 1** Average distances between centers of mass of the residues at the HAC PD-1/PD-L1 interface for two pH levels

| Binding pocket residues (PD-1 - PD-L1) | Average distance, Å Blood pH | Average distance, Å Acidic pH |
|---|---|---|
| His68-Asp122 | 2.21 ± 0.15 | 1.85 ± 0.02 |
| Thr78-Asp122 | 2.52 ± 0.44 | 2.19 ± 0.05 |
| Glu136-Tyr123 | 3.07 ± 0.11 | 2.71 ± 0.09 |
| Glu136-Arg125 | 5.34 ± 2.10 | 6.31 ± 3.3 |
| Glu70-Arg125 | 4.02 ± 2.23 | 5.53 ± 3.1 |

To estimate the binding rate ($k_{on}$) and dissociation ($K_d$) constants, we complimented our metadynamics calculations with umbrella sampling simulations. The binding rate $k_{on}$ was estimated from the binding energy ($\Delta G$) and unbinding rate constant ($k_{off}$) assuming two-state kinetics.[22] A PD-L1 ligand was pulled along the reaction coordinate (the distance between centers of mass for the binding pockets of PD-1 and PD-L1) with a velocity of 0.01 nm·ns$^{-1}$ and a force constant of 1000 kJ·mol$^{-1}$·nm$^2$. From this steered MD trajectory, 12 windows were extracted for the umbrella sampling with spacing between adjacent windows of 0.1 nm (from 0.7 to 1.8 nm along the reaction coordinate). The system in each window was then equilibrated for 10 ns, followed by a 30-ns production run (the force constant was set to 3000 kJ·mol$^{-1}$·nm$^2$). The potential of mean force was calculated using the weighted histogram analysis method[24] as implemented in the Gromacs 2016.3 package.

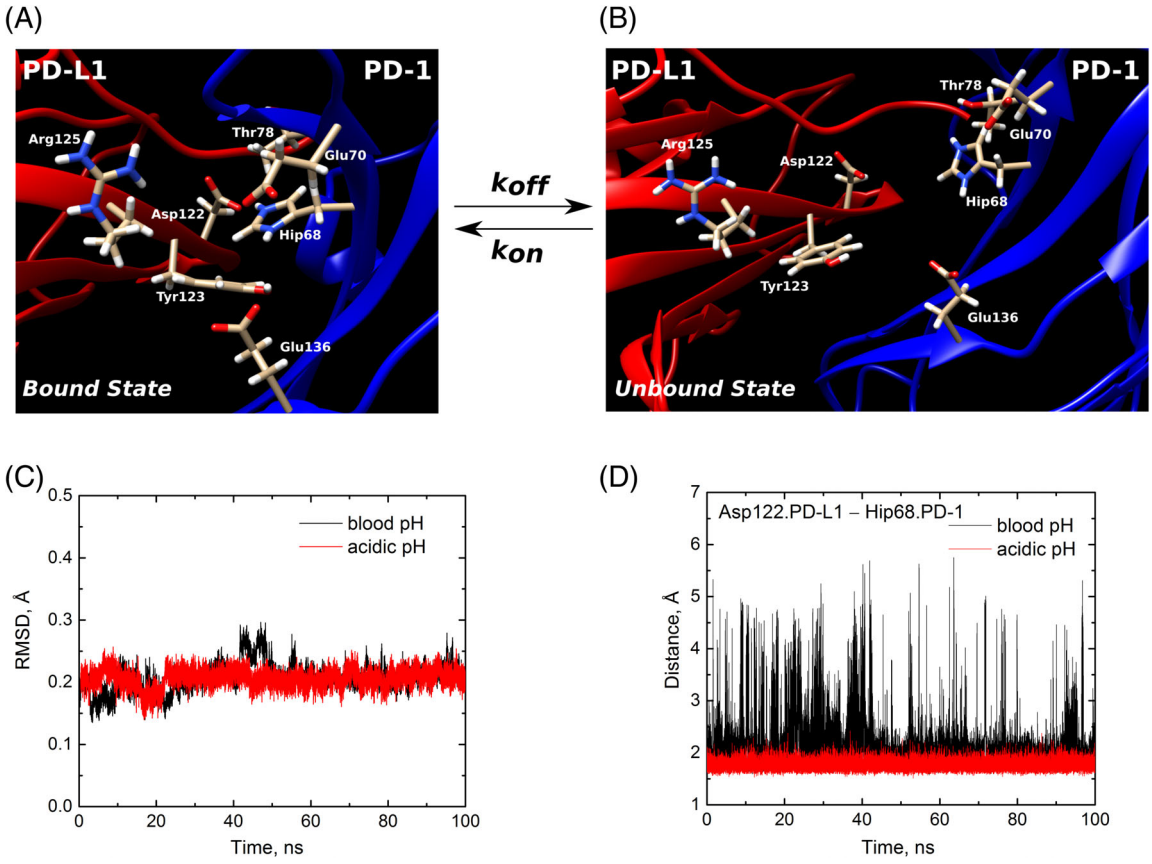


**FIGURE 2** Structure of the HAC PD-1/PD-L1 binding pocket in the (A) bound state and (B) unbound state. C, Root mean square deviations from molecular dynamics trajectories for all the non-hydrogen atoms in the PD-1/PD-L1 complex and (D) evolution of distances between the N group of Hip68 in PD-1 and O of Asp122 in PD-L1 for blood and acidic pH levels [Color figure can be viewed at wileyonlinelibrary.com]

## 3 | RESULTS AND DISCUSSION

To examine the binding properties of the PD-1/PD-L1 protein-ligand pair, we choose a recently engineered ultra-high-affinity mutant of PD-1 (HAC) that exhibits up to 40 000-fold enhanced affinity for PD-L1 relative to the wild-type human PD-1.[13] An X-ray crystallographic analysis of the HAC PD-1/PD-L1 complex was previously carried out to obtain the atomic structure with a 2.9 Å resolution (PDB ID: 5IUS).[13] It was shown that the crystallized complex exhibits a 2:2 binding stoichiometry, whereas in solution the complex was confirmed to have a 1:1 stoichiometry that is chosen for the present study (see Figure 1). The missing residues were recovered using the Modeller software[14] to make both halves of the protein identical. To assign protonation states of the titratable residues, we use p$K_a$ values obtained in the propKa software.[15] The protonation states are determined for the two representative pH levels: pH 5.5 mimicking the extracellular environment of tumors[25-27] and pH 7.4 corresponding to normal tissues.[27] In this study, we define these pH levels as acidic pH and blood pH, respectively.

Our analysis of the protonation diagram for the PD-1/PD-L1 complex indicates that several amino acids (namely, His64, His68, and His107 of PD-1, and Glu58, and His78 of PD-L1) should change the protonation states in the pH range of 5.5-7.4 based on their p$K_a$ values (see Movie S1 for more details). Figure 2 depicts the atomic structures of the binding pocket for the PD-1/PD-L1 complex in both bound (A) and unbound (B) configurations. Figure 2C shows the time evolution of the root mean square deviation over a 100 ns MD production trajectory for the bound state (BS; A) demonstrating stability of the complex under both pH conditions.

We next identify the residue interaction network formed at the interface between PD-1 and PD-L1. In agreement with previous studies,[28] our calculations show that the binding pocket between PD-1 and PD-L1 is primarily comprised of His68, Glu70, Thr78, and Glu136 from the PD-1 side and Asp122, Tyr123, Arg125, and Lys124 from the PD-L1 side (see Figure 2 for the overall structure and Table 1 for the average distances between the residues). While other residues should also contribute to the complex stability, the distances between the corresponding hot spots are found to fluctuate quite significantly suggesting much weaker interactions. The computed average distances between the residues in the binding pocket (Table 1) indicate that the stability of the PD-1/PD-L1 complex indeed depends on the considered pH level. For example, it is seen that the distance between protonated His68.PD-1 and Asp122.PD-1 decreases from around 2.21 Å under circumneutral conditions to 1.85 Å in acidic environment. The interaction between Thr78.PD1 and Asp122.PD-L1 also contributes to the stability of the binding configuration but are characterized by larger average distances. Based on this structural information, it is clear that pH changes have an effect on binding interactions whose strength will be quantified below using free energy calculations.

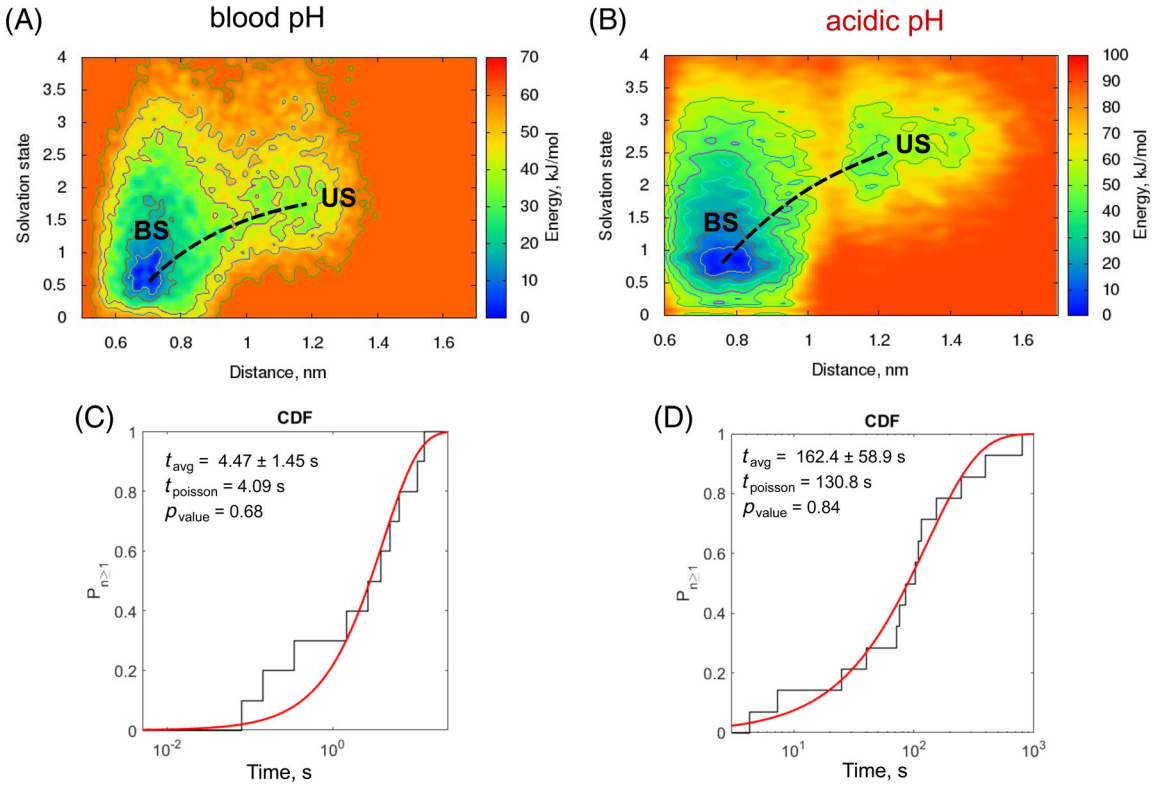


**FIGURE 3** A and B, Representative two-dimensional free energy surfaces for unbinding process as a function of distance between PD-1 and PD-L1 and solvation state of the binding pocket. Bound and unbound states are shown in Figure 2A,B and stand for bound and unbound states, correspondingly. C and D, Cumulative distribution functions (CDF) for unbinding times fitted as a Poisson process for two pH levels [Color figure can be viewed at wileyonlinelibrary.com]

Having equilibrated the PD-1/PD-L1 system in the BS, we next undertake kinetic simulations employing enhanced sampling free energy methods. First, we examine the unbinding process by means of metadynamics approach based on an infrequent deposition of the repulsive Gaussians in the CV space.[20,21] By using the distance between the centers of mass of the residues from the PD-1/PD-L1 binding pocket as CV1 and solvation state of the ligand as CV2 (see Section 2), we investigate the free energy landscape of PD-1/PD-L1 unbinding and directly compute the residence time of the protein-ligand pair in the BS. The combination of these two CVs was previously demonstrated to be important for accurate description of the protein-ligand unbinding process in metadynamics.[23]

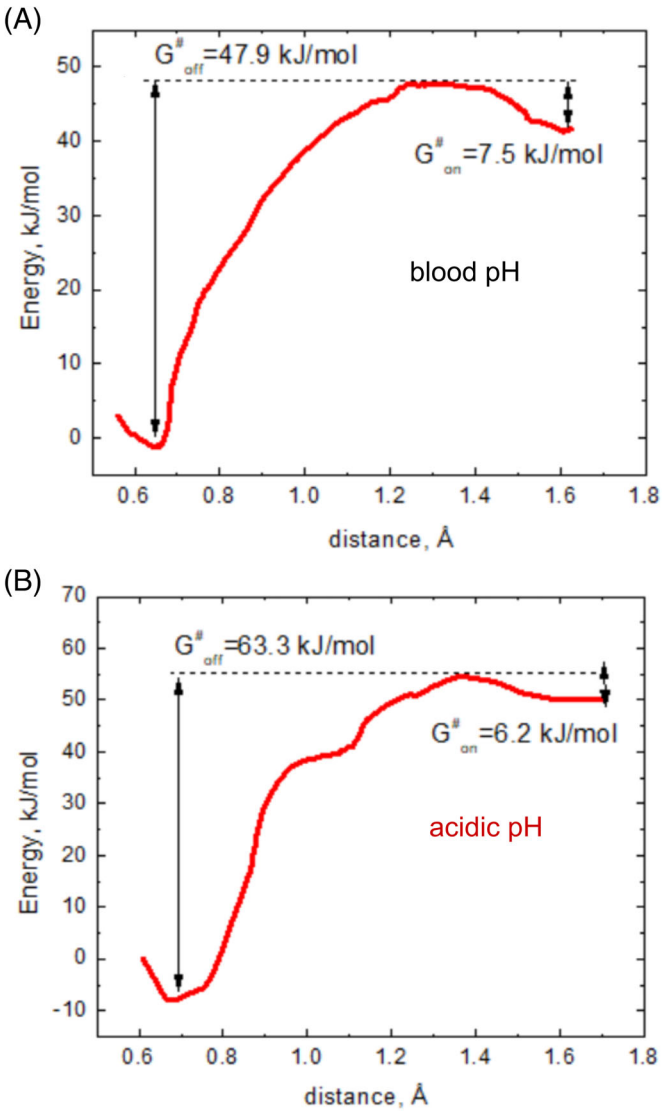


**FIGURE 4** Free energy profiles of PD-1 and PD-L1 binding as computed in umbrella sampling for (A) blood pH and (B) acidic pH [Color figure can be viewed at wileyonlinelibrary.com]

The representative free energy maps for unbinding process for acidic and blood pH levels are shown in Figure 3, while Movie S1 illustrates the simulated dynamics of unbinding reaction. It is found that the BS for both pH cases is characterized by the CV1 value of ~0.7 nm and minimal solvation (CV2) that can include one water molecule on average due to spontaneous destabilization of bonds between several hot spots as discussed above. Upon unbinding, water molecules enter the binding pocket space leading to an increase in distances between the hot spots. After CV1 reaches ~1.2 nm, the system falls into the basin of the US, as seen from Figure 3A,B. In this US, the hot spots of both the protein and the ligand are solvated and separated from each other by several water molecules. After reaching the US, the ligand diffuses easily either into the solvent or back to the protein (as shown in Movie S1). The average activation barriers for the unbinding process as estimated from metadynamics are 44 ± 7 kJ/mol for circumneutral pH and 57 ± 10 kJ/mol for acidic pH.

We next evaluate the lifetimes for the PD-1/PD-L1 pair in the bound pose at different pH levels over multiple state-to-state (BS → US) metadynamics trajectories using acceleration factor as described in Section 2 and shown in Movie S1. The average unbinding time is computed by fitting the obtained distribution of residence times in the BS with a Poisson function (see Figure 3C,D). We find $t_{poisson}$ to be 4.09 and 130.8 seconds, resulting in unbinding rate constants ($k_{off}$) of 0.24 second$^{-1}$ and 7.6·10$^{-3}$ second$^{-1}$ for blood and acidic pH, respectively. The reliability of residence time statistics is analyzed using the Kolmogorov-Smirnov test yielding the *P* values of .68 and .84 thereby confirming that the distribution is Poissonian. Thus, our results reveal two orders of magnitude difference in $k_{off}$ between blood and acidic pH. This is in qualitative agreement with recent experimental estimates that, however, result in smaller $k_{off}$ values.[13]

In order to evaluate the thermodynamic equilibrium dissociation constant ($K_d = k_{off}/k_{on}$), we need to obtain $k_{on}$ values by simulating the binding process between PD-1 and PD-L1. Such simulations within the metadynamics approach can be rather computationally challenging as the system in the US has the flexibility of exploring a multitude of possible solvated states that may frustrate evaluation of binding

**TABLE 2** Comparison of simulated and experimental data on the rate constants for HAC PD-1/PD-L1

| | Simulation | | Experiment[13] | |
|---|---|---|---|---|
| | Blood pH | Acidic pH | Blood pH | Acidic pH |
| $k_{off}$, $s^{-1}$ | 0.24 | 7.6·10$^{-3}$ | 3.4·10$^{-4}$ | Not measurable |
| $k_{on}$, 106 $M \cdot s^{-1}$– | 27.57 | 1061.31 | 2.61 | 118 |
| $K_d$, pM | 12 404.36 | 6.69 | 127 | – |

*Note*: Experimental values are taken from Ref.[13] and correspond to pH 7.4 and 5.5 for blood and acidic pH levels, respectively.

free energies. To improve the efficiency of sampling of the ligand/protein binding pathway, a number of approaches[29] have been previously employed including Brownian dynamics,[30] funnel metadynamics,[31] and thermodynamic integration.[22,32] Here, to estimate the binding rate constants, we choose to apply the umbrella sampling technique[24] (see Section 2 for more details). To compute the free energy profiles of the binding process, the distance between centers of masses of the protein and its ligand residues in the binding pocket is chosen as the CV, similarly to CV1 in our metadynamics simulations.

Figure 4 shows the simulated free energy profiles of the reaction for two pH levels. The computed unbinding free energy barriers of 47.9 and 63.3 kJ/mol for blood and acidic pH, respectively, agree fairly well with the metadynamics estimates (44 ± 7 and 57 ± 10 kJ/mol, correspondingly). This allows us to conclude that relatively large equilibration times for each window in umbrella sampling simulations helped improve solvation of the binding pocket and force averaging to estimate the binding affinity with a single CV. The activation barriers of binding are computed to be 7.5 and 6.2 kJ/mol for circumneutral and acidic pH, correspondingly. In addition, the free energy difference $\Delta G$ of −40.4 kJ/mol between the BS and US at neutral pH agrees very well with the value of −43.1 kJ/mol estimated using isothermal calorimetry on the HAC PD-1/PD-L1 system.[13] These calorimetric measurements have also demonstrated that the binding process between HAC PD-1 and PD-L1 is enthalpically driven, in contrast to the results obtained for the wild-type proteins. Using the computed binding energy, we then estimate the $k_{on}$ values for a standard reference concentration of 1 M assuming two-state kinetics. Finally, the dissociation constant $K_d$ is assessed for both pH levels as presented in Table 2. Overall, the obtained computational results posit strong pH sensitivity of the PD-1/PD-L1 binding kinetics, in overall agreement with recent experimental studies.

## 4 | CONCLUSIONS

Using atomistic MD simulations, we have provided atomistic insights into the mechanism of PD-1/PD-L1 interaction and demonstrated that pH level could significantly affect the binding affinity of immune checkpoint proteins. In particular, we have shown that electrostatic interactions between the His-68.PD-1 and Asp122.PD-L1 residues give a significant contribution to binding affinity, with protonation state of imidazole ring playing a key role in protein binding/unbinding process. Our computational findings are in good qualitative agreement with recent experimental measurements,[13] while the absolute binding/unbinding rates are overestimated (see Table 2).

The discrepancy between calculated and experimental residence times could be due to several factors. First, the protonation states of binding counterparts are fixed during simulation trajectories, while under real experimental conditions there must be a dynamic equilibrium. p$K_a$ values of titratable groups are typically determined by empirical prediction methods that are unable to capture the dynamics of protonation state changes arising as a response to the occurring reaction and possible conformational changes. Another set of uncertainties was shown to be inherent to the computational methods employed to evaluate binding/unbinding kinetics[29,33] and includes errors associated with the choice of CVs to sample free energy landscape of a reaction, as well as approximations related to the applied classical force fields. The use of quantum chemical calculations to treat regions associated with active binding sites, for example, within the hybrid quantum mechanics/molecular mechanics approach could improve accuracy of kinetic simulations.

Based on the ability of employed computational methods to provide a qualitatively correct picture of the pH-sensitive binding for immune checkpoint proteins, this study should serve as a good starting point for the development of more efficient immune checkpoint blockade strategies based on pH dependent interaction between proteins and their ligands. Introduction of more histidine residues in the binding pocket emerges as a natural choice for tuning pH-dependent binding equilibrium and can also help explain variable patient responses to immunotherapies. It is expected that with the aid of available libraries of biocompatible scaffold proteins, the hotspot interfaces with desired pH-sensitive molecular footprints could be designed using computational screening methods.[34]

## ACKNOWLEDGMENTS

The Holland Computing Center at the University of Nebraska-Lincoln is acknowledged for computational support.

## REFERENCES

1. Sharma P, Allison JP. The future of immune checkpoint therapy. *Science*. 2015;348(6230):56-61.
2. Sharma P, Allison JP. Immune checkpoint targeting in cancer therapy: toward combination strategies with curative potential. *Cell*. 2015;161(2):205-214.
3. Topalian SL, Drake CG, Pardoll DM. Immune checkpoint blockade: a common denominator approach to cancer therapy. *Cancer Cell*. 2015;27(4):450-461. https://doi.org/10.1016/j.ccell.2015.03.001.
4. Wei SC, Duffy CR, Allison JP. Fundamental mechanisms of immune checkpoint blockade therapy. *Cancer Discov*. 2018;8(9):1069-1086. https://doi.org/10.1158/2159-8290.CD-18-0367.
5. Khalil DN, Smith EL, Brentjens RJ, Wolchok JD. The future of cancer treatment: immunomodulation, CARs and combination immunotherapy. *Nat Rev Clin Oncol*. 2016;13(5):273-290. https://doi.org/10.1038/nrclinonc.2016.25.
6. Hoos A. Development of immuno-oncology drugs—from CTLA4 to PD1 to the next generations. *Nat Rev Drug Discov*. 2016;15(4):235-247. https://doi.org/10.1038/nrd.2015.35.
7. Petukh M, Stefl S, Alexov E. The role of protonation states in ligand-receptor recognition and binding. *Curr Pharm des*. 2013;19(23):4182-4190. https://doi.org/10.2174/1381612811319230004.
8. Lee J, Miller BT, Brooks BR. Computational scheme for pH-dependent binding free energy calculation with explicit solvent. *Protein Sci*. 2016;25(1):231-243. https://doi.org/10.1002/pro.2755.
9. Watanabe S, Harayama M, Kanemura S, Sitia R, Inaba K. Structural basis of pH-dependent client binding by ERp44, a key regulator of protein secretion at the ER-Golgi interface. *Proc Natl Acad Sci*. 2017;114(16):E3224-E3232. https://doi.org/10.1073/pnas.1621426114.
10. Igawa T, Ishii S, Tachibana T, et al. Antibody recycling by engineered pH-dependent antigen binding improves the duration of antigen neutralization. *Nat Biotechnol*. 2010;28(11):1203-U96. https://doi.org/10.1038/nbt.1691.

11. Devanaboyina SC, Lynch SM, Ober RJ, et al. The effect of pH dependence of antibody-antigen interactions on subcellular trafficking dynamics. *MAbs*. 2013;5(6):851-859. https://doi.org/10.4161/mabs.26389.
12. Lázár-Molnár E, Scandiuzzi L, Basu I, et al. Structure-guided development of a high-affinity human programmed cell death-1: implications for tumor immunotherapy. *EBioMedicine*. 2017;17:30-44.
13. Pascolutti R, Sun X, Kao J, et al. Structure and dynamics of PD-L1 and anultra-high-affinity PD-1 receptor mutant. *Structure*. 2016;24(10):1719-1728.
14. Eswar N, Webb B, Marti-Renom MA, et al. Comparative protein structure modeling using modeller. *Curr Protoc Bioinformatics*. 2006;15(1):5-6.
15. Olsson MH, Søndergaard CR, Rostkowski M, Jensen JH. PROPKA3: consistent treatment of internal and surface residues in empirical pKa predictions. *J Chem Theory Comput*. 2011;7(2):525-537.
16. Berendsen vdSD, Drunen vR. GROMACS: a message-passing parallel molecular dynamics implementation. *Comput Phys Commun* 1995; 91 (1–3): 43–56.
17. Duan Y, Wu C, Chowdhury S, et al. A point-charge force field for molecular mechanics simulations of proteins based on condensed-phase quantum mechanical calculations. *J Comput Chem*. 2003;24 (16):1999-2012.
18. Bussi G, Donadio D, Parrinello M. Canonical sampling through velocity rescaling. *J Chem Phys*. 2007;126(1):014101.
19. Parrinello M, Rahman A. Polymorphic transitions in single crystals: a new molecular dynamics method. *J Appl Phys*. 1981;52(12):7182-7190.
20. Bonomi M, Branduardi D, Bussi G, et al. PLUMED: a portable plugin for free-energy calculations with molecular dynamics. *Comput Phys Commun*. 2009;180(10):1961-1972.
21. Tiwary P, Parrinello M. From Metadynamics to dynamics. *Phys Rev Lett*. 2013;111(23):230602.
22. Wang Y, Martins JM, Lindorff-Larsen K. Biomolecular conformational changes and ligand binding: from kinetics to thermodynamics. *Chem Sci*. 2017;8(9):6466-6473.
23. Tiwary P, Mondal J, Berne BJ. How and when does an anticancer drug leave its binding site? *Sci Adv*. 2017;3(5):e1700014.
24. Kumar S, Rosenberg JM, Bouzida D, Swendsen RH, Kollman PA. The weighted histogram analysis method for free-energy calculations on biomolecules. I. the method. *J Comput Chem*. 1992;13(8):1011-1021.
25. Estrella V, Chen T, Lloyd M, et al. Acidity generated by the tumor microenvironment drives local invasion. *Cancer Res*. 2013;73(5):1524-1535.
26. Gatenby RA, Gillies RJ. Why do cancers have high aerobic glycolysis? *Nat Rev Cancer*. 2004;4(11):891.
27. Vaupel P, Kallinowski F, Okunieff P. Blood flow, oxygen and nutrient supply, and metabolic microenvironment of human tumors: a review. *Cancer Res*. 1989;49(23):6449-6465.
28. Shi D, Zhou S, Liu X, Zhao C, Liu H, Yao X. Understanding the structural and energetic basis of PD-1 and monoclonal antibodies bound to PD-L1: a molecular modeling perspective. *Biochim Biophys Acta*. 2018;1862(3):576-588.
29. Bruce NJ, Ganotra GK, Kokh DB, Sadiq SK, Wade RC. New approaches for computing ligand–receptor binding kinetics. *Curr Opin Struct Biol*. 2018;49:1-10.
30. Zeller F, Luitz MP, Bomblies R, Zacharias M. Multiscale simulation of receptor–drug association kinetics: application to neuraminidase inhibitors. *J Chem Theory Comput*. 2017;13(10):5097-5105.
31. Moraca F, Amato J, Ortuso F, et al. Ligand binding to telomeric G-quadruplex DNA investigated by funnel-metadynamics simulations. *Proc Natl Acad Sci*. 2017;114(11):E2136-E2145.
32. Woo HJ, Roux B. Calculation of absolute protein–ligand binding free energy from computer simulations. *Proc Natl Acad Sci*. 2005;102(19):6825-6830.
33. Ribeiro JML, Tsai ST, Pramanik D, Wang Y, Tiwary P. Kinetics of ligand–protein dissociation from all-atom simulations: are we there yet? *Biochemistry*. 2018;58(3):156-165.
34. Lavecchia A, Di Giovanni C. Virtual screening strategies in drug discovery: a critical review. *Curr Med Chem*. 2013;20(23):2839-2860.


## SUPPORTING INFORMATION

Additional supporting information may be found online in the Supporting Information section at the end of this article.

**How to cite this article:** Klyukin K, Alexandrov V. Kinetics of pH-dependent interactions between PD-1 and PD-L1 immune checkpoint proteins from molecular dynamics. *Proteins*. 2020; 88:1162–1168. https://doi.org/10.1002/prot.25885